Interstitial Superstructures in the Ta–D System

H. ASANO, Y. ISHINO, R. YAMADA,* AND M. HIRABAYASHI

The Research Institute for Iron, Steel and Other Metals, Tohoku University, Sendai 980, Japan

Ordered deuterium arrangements and order–disorder transformations of the tantalum deuterides in the range $TaD_{0.50}$–$TaD_{0.78}$ have been studied by neutron diffraction and calorimetry at temperatures between −170 and 120°C. In addition to the disordered phase (α), three ordered phases based on the superstructures Ta_2D_{1+x} (β_1), Ta_4D_3 (γ), and TaD (δ) are clarified. The Ta_2D_{1+x} structure is a nonstoichiometric form of the Ta_2D superstructure over the range $x < 0.5$. The γ-phase is formed below −70°C near Ta_4D_3, and transforms into the β_1 and δ-phases, respectively, in the hypo and hyperstoichiometric compositions. The δ-phase that exists beyond $TaD_{0.75}$ changes to the disordered α-phase around 100°C.

1. Introduction

The Ta–H(D) alloy is known as an interstitial solid solution of hydrogen (deuterium) in bcc tantalum. According to the phase diagram proposed by Waite et al. (*1*), the Ta–H system contains two phases, α and β. The high-temperature α-phase decomposes into α and β below about 50°C. At room temperature the α-phase extends up to $TaH_{0.2}$, the ($\alpha + \beta$) two-phase field exists in the range $TaH_{0.2}$–$TaH_{0.5}$ and the β-phase with a monoclinic metal lattice (*2, 3*) exists beyond $TaH_{0.5}$.

The ordered deuterium arrangements in the Ta–D alloy studied by neutron diffraction have been reviewed by Somenkov (*4*). There exist three superstructures, Ta_2D (*5*), Ta_4D_3 (*6*), and TaD (*7*). These structures, shown in Fig. 1, are closely related to each other; the framework of the metal atoms is the same and the deuterium atoms are ordered in the specific tetrahedral sites. (Although the metal lattice is monoclinic, the alloy appears to be cubic in the powder neutron diffraction patterns due to its poor resolution.)

* Present address: Japan Atomic Energy Research Institute, Tokai, Ibaraki 319–11, Japan.

The structures of Ta_2D and Ta_4D_3 are derived by subtracting regularly the deuterium atoms from the TaD structure. The TaD structure has been found only in the nonstoichiometric compositions $TaD_{0.75}$ (*6*) and $TaD_{0.87}$ (*7*) at room temperature, and the Ta_4D_3 superstructure is formed in the low temperature region of the β-phase (*6*).

However, at present, phase relations among these ordered phases are not well-established. Detailed information on the order–disorder transformation is also lacking. The present work [a preliminary result of which has been presented in (*8*)] is undertaken to reveal the variation of the deuterium arrangement with composition in the range $TaD_{0.50}$–$TaD_{0.78}$ and the order–disorder transformation of each superstructure by means of neutron diffraction and calorimetry.

2. Experimental

The Ta–D alloys with the compositions $TaD_{0.50}$–$TaD_{0.78}$ were prepared by the reaction of tantalum powder with deuterium gas using a Sieverts' type apparatus. The method of preparation was the same as previously reported (*9*). X-ray diffraction

45
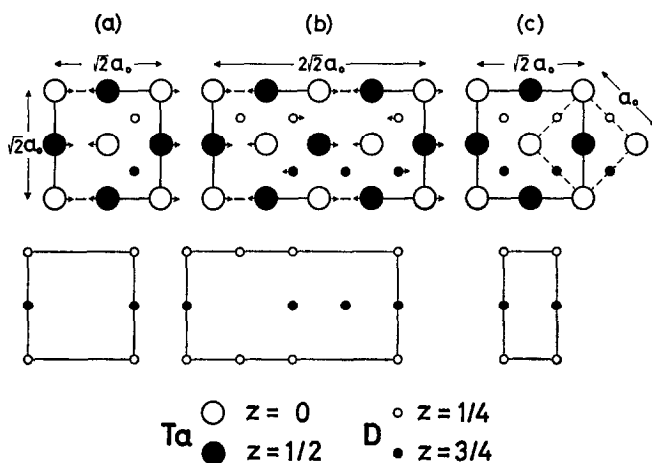
FIG. 1. Superstructures of (a) Ta_2D, (b) Ta_4D_3, and (c) TaD. The pseudocubic metal lattice with the parameter a_0 is drawn by dashed lines in (c). The atomic displacements in Ta_2D and Ta_4D_3 are indicated by arrows. The deuterium sublattice of each structure is shown in the lower part.
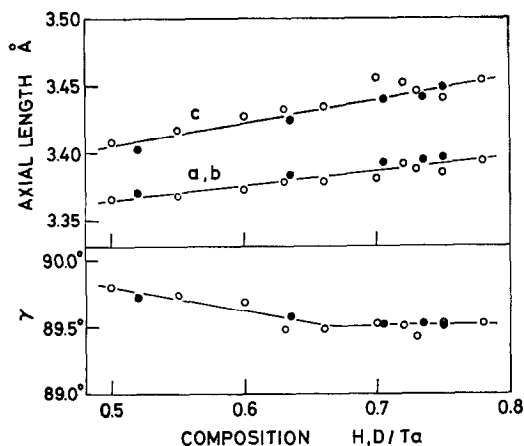
FIG. 2. Lattice parameters of the Ta–D alloys. o, present work; ●, results for the Ta–H alloys (2). The parameters a (=b) and c are determined from 400 and 004 reflections, respectively, and γ is deduced from the line-splitting of 222 reflection. A 114.6-mm camera and Cu$K\alpha$ radiation are used.

patterns taken at room temperature showed all the samples to be monoclinic in accordance with the previous work on the Ta–H system (2, 3). The lattice parameters are shown in Fig. 2 with the results for the hydrides (2). Neutron diffraction experiments were carried out at temperatures between −170 and 110°C using the TOG diffractometer at the JRR-3

reactor of JAERI. The neutron wavelength was close to 1.0 Å. Heat capacity measurements were made on heating from −140–120°C using an adiabatic calorimeter.

3. Results

3.1. Structure of Ta_2D_{1+x}

As mentioned above, Petrunin et al. (5) have determined the superstructure Ta_2D at the stoichiometric composition. To elucidate the deuterium arrangement in the nonstoichiometric region, neutron diffraction experiments are made on $TaD_{0.60}$ and $TaD_{0.72}$ at room temperature. The observed diffraction patterns are analogous to the previous results on Ta_2D (5, 10). As shown in Fig. 3, the structure is described by the same unit cell ($A = C = (2)^{1/2}a_0, B = a_0$) and space group ($C222$) as those of the Ta_2D structure (5). The atomic arrangement of Ta_2D_{1+x} is determined as

$$(0\ 0\ 0, \tfrac{1}{2}\tfrac{1}{2}0) +$$

4 Ta in 4(k): $\tfrac{1}{4}\tfrac{1}{4}z, \tfrac{1}{4}\tfrac{3}{4}\bar{z}$ with $z = \tfrac{3}{4} - \Delta$

2x D in 2(d): $0\ 0\ \tfrac{1}{2}$

2 D in 2(a): $0\ 0\ 0,$
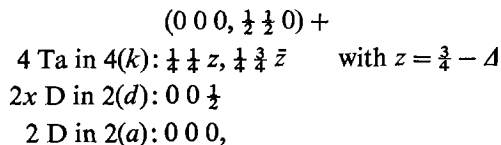
where Δ indicates the atomic displacement shown by arrows in Fig. 3. This structure is a nonstoichiometric form of Ta_2D with the
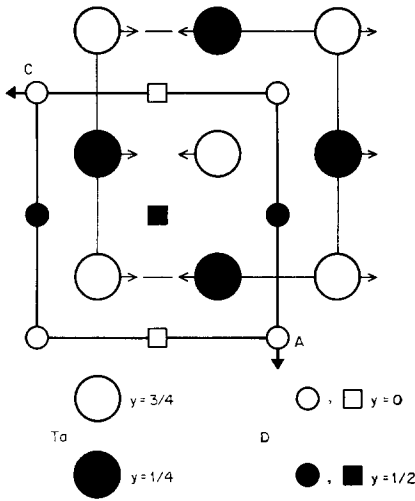
FIG. 3. Superstructure of Ta_2D_{1+x}. The tetrahedral sites marked with □ and ■ are partly filled by the excess deuterium atoms with the probability x.

statistical occupation of the excess deuterium atoms in the $2(d)$ sites. A comparison of the observed and calculated intensities is given in Table I, R-factors

$$\left(\text{defined as } \sum |I_{obs} - I_{cal}|/\sum I_{obs}\right)$$

being 0.04 and 0.06, respectively, for $TaD_{0.60}$ and $TaD_{0.72}$. Hereafter, the phase with the Ta_2D_{1+x} structure is termed as β_1. The

deuterium-rich limit of the β_1-phase at room temperature is considered to lie near $TaD_{0.74}$, since the TaD structure (δ) appears at $TaD_{0.75}$ according to (6).

3.2. Heat Capacity Measurements

Figure 4 shows the heat capacity curve of Ta_2D, exhibiting a sharp peak at 58°C and a subsidiary hump around 54°C. The result is somewhat different from the heat capacity data of Ta_2H (11), which show three thermal anomalies at 33, 59, and 60°C, corresponding to the stepwise transitions $\beta_1-\beta_2-\beta_3-\alpha$. From the analogy of Ta_2H, the hump of 54°C observed in Ta_2D may correspond to the $\beta_1-\beta_2$ transition, concerning which discussion is made later.

In the heat capacity curves of $TaD_{0.55}$, $TaD_{0.60}$, and $TaD_{0.63}$, the hump due to the $\beta_1-\beta_2$ transition is no longer observed and the $\beta_1-\alpha$ transition occurs in a single step. Figure 5 shows the specific heat curve and the temperature dependence of neutron diffraction intensities of $TaD_{0.60}$. The intensities of the superlattice reflections 001 and 110 decrease with increasing temperature and disappear at 56°C, and hence, the $\beta_1-\alpha$ transition is attributed to the disordering of the Ta_2D_{1+x} structure.

As shown in Fig. 6, the result of $TaD_{0.66}$

TABLE I

COMPARISON OF THE OBSERVED AND CALCULATED INTENSITIES OF β_1-$TaD_{0.60}$ AND β_1-$TaD_{0.72}$ AT ROOM TEMPERATURE[a]

HKL	$TaD_{0.60}$ ($x = 0.20$)		$TaD_{0.72}$ ($x = 0.44$)	
	I_{obs}	I_{cal}	I_{obs}	I_{cal}
001	7.7	6.2	2.3	2.6
110	15.6	14.4	25.5	22.7
111,002,200	100.0	100.0	100.0	100.0
201	4.9	5.4	0.7	3.4
112	13.5	12.3	20.2	19.3
202,020	49.0	46.2	64.0	57.4
003,021	5.7	5.6		

[a] Δ is assumed to be 0.012 according to (5), and the Debye–Waller factors $B_{Ta} = 0.3$ Å² and $B_D = 1.3$ Å² are used.

FIG. 4. Specific heat curve of $TaD_{0.50}$. Heat capacity is referred to the alloy containing 1 mole of Ta.

again shows a double peak. With increasing deuterium content the high-temperature anomaly becomes dominant and shifts to higher
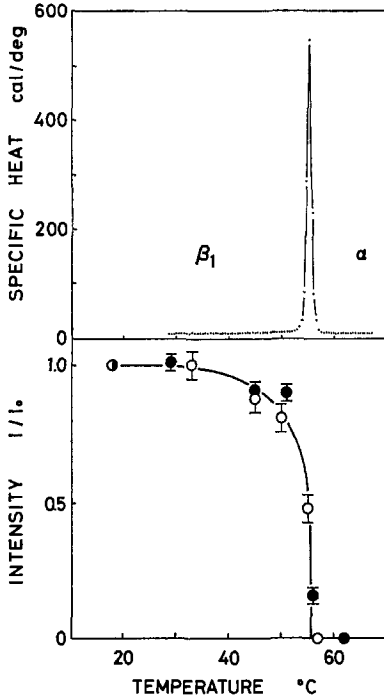
FIG. 5. Specific heat and superlattice reflection intensities versus temperature curves of $TaD_{0.60}$. O and ● represent 001 and 110 reflections, respectively, and I_0 is the intensity at 18°C.

temperatures, while the low-temperature one, whose peak height becomes smaller, appears at a constant temperature (56°C) up to $TaD_{0.72}$ and disappears in $TaD_{0.75}$. The high-temperature X-ray diffractometry shows that the intermediate region between the two anomalies corresponds to the two-phase mixture of the cubic α-phase and the monoclinic δ-phase. This also is confirmed by the neutron diffraction study described in the next section. The alloys $TaD_{0.75}$ and $TaD_{0.78}$ with the TaD superstructure (δ) at room temperature (6, 7) undergo the δ–α transition near 100°C.

Figure 7 shows the specific heat curves of the alloys near Ta_4D_3 below room temperature. Anomalous heat absorptions are observed around −70°C, which are shown in the next section to be due to the first step transition in the successive disordering of the Ta_4D_3 superstructure (γ).

3.3. Order–Disorder Transformation of Ta_4D_3

Somenkov et al. (6) have studied the order–disorder transformation of $TaD_{0.75}$ by neutron diffraction and reported that the Ta_4D_3 superstructure transforms to the TaD structure at −20°C. As seen in Figs. 6d and 7b, the specific heat curve of $TaD_{0.75}$ shows two thermal anomalies at −75 and 94°C, but no
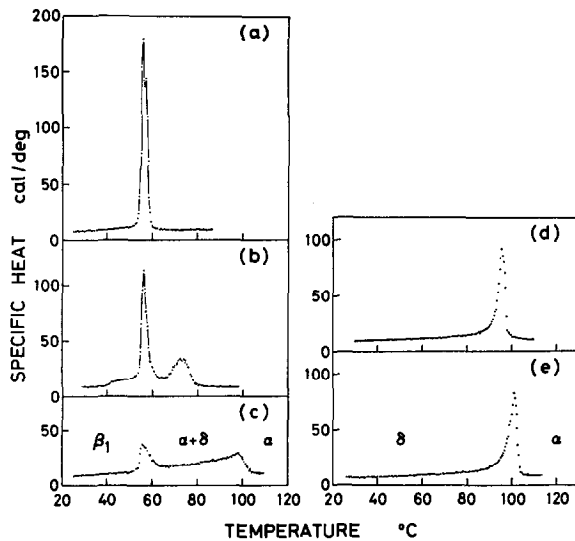
FIG. 6. Specific heat curves of (a) $TaD_{0.66}$, (b) $TaD_{0.70}$, (c) $TaD_{0.72}$, (d) $TaD_{0.75}$, and (e) $TaD_{0.78}$.
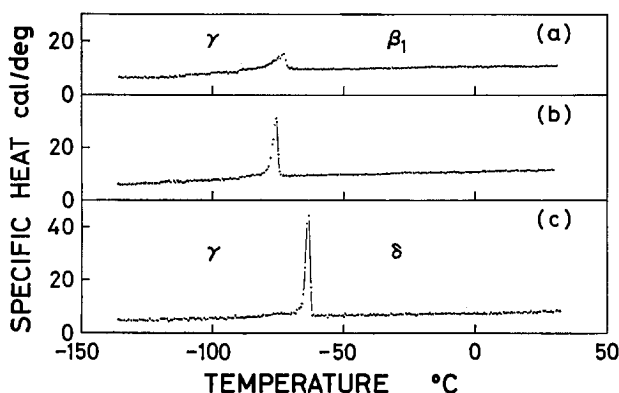
FIG. 7. Specific heat curves of (a) $TaD_{0.72}$, (b) $TaD_{0.75}$, and (c) $TaD_{0.78}$ at low temperatures.

anomaly is seen around −20°C. Moreover, the result of $TaD_{0.72}$ (Figs. 6c and 7a) shows the stepwise phase transitions $\gamma-\beta_1-(\alpha + \delta)-\alpha$ at −73, 56, and 98°C, which is inconsistent with the proposal of Somenkov et al. (6).

To clarify the reason for these discrepancies, neutron diffraction experiments were made on $TaD_{0.72}$ at temperatures from −166–110°C. The result obtained at −166°C (γ-phase) is interpreted well by the Ta_4D_3 superstructure (6) with the unit cell of $A = (2)^{1/2}a_0$, $B = 2(2)^{1/2}a_0$, and $C = a_0$ and the space group $I222$:

$$(0\ 0\ 0, \tfrac{1}{2}\,\tfrac{1}{2}\,\tfrac{1}{2}) +$$

8 Ta in 8(k): xyz, $\bar{x}\bar{y}z$, $x\bar{y}\bar{z}$, $\bar{x}y\bar{z}$

with $x = \tfrac{1}{4}$, $y = \tfrac{1}{8} - \Delta'$, $z = \tfrac{3}{4}$

4 D in 4(g): $0y0$, $0\bar{y}0$ with $y = \tfrac{1}{4} + \Delta''$

1.76 D in 2(a): 000,

where Δ' and Δ'' are the atomic displacements of tantalum and deuterium, respectively, shown by arrows in Fig. 1b. The observed and calculated intensities are compared in Table II, with R-factor 0.10. It is concluded, therefore, that the γ-phase is based on the Ta_4D_3 superstructure.

Temperature variations of the superlattice reflection intensities are shown in Fig. 8. These reflections are classified into three groups: (I) with $K =$ odd (Fig. 8a), (II) with $K = 4n + 2$ (Fig. 8b), and (III) with $K = 4n$ (Fig. 8c), which are characteristic of the Ta_4D_3, Ta_2D_{1+x}, and TaD structures, respectively. [The classification is based on the

fact that the deuterium sublattices of the Ta_2D_{1+x} and TaD structures are respectively $\tfrac{1}{2}$ and $\tfrac{1}{4}$ of that of the Ta_4D_3 structure along the B-axis (see Fig. 1). The following relations among the indices of the three superstructures hold; $H'K'L' = HLK/2$ and $H''K''L'' = K/2$ HL, where HKL, $H'K'L'$ and $H''K''L''$ are the indices of the Ta_4D_3, Ta_2D_{1+x} and TaD structures, respectively.] As shown in Fig. 8a, the type I reflections vanish at the temperature where the $\gamma-\beta_1$ transition occurs in the specific heat curve of Fig. 7a. It is evident, therefore,

TABLE II

COMPARISON OF THE OBSERVED AND CALCULATED INTENSITIES OF γ-$TaD_{0.72}$ AT −166°C[a]

HKL	I_{obs}	I_{cal}
020	4.2	3.2
110	1.1	3.8
011	2.2	2.1
101	27.6	22.7
130	0.8	4.0
121, 040, 200	} 103.0	100.0
031		3.0
220	1.1	2.9
211	0.8	1.4
141	} 23.7	24.5
150		0.1
240, 002	65.9	57.3

[a] The parameters are assumed as $\Delta' = 0.004$ and $\Delta'' = 0.01$ according to (6), and the Debye–Waller factors $B_{Ta} = 0.1$ Å^2 and $B_D = 0.8$ Å^2 are used.
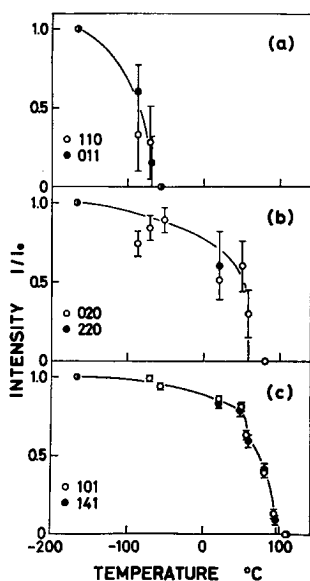
FIG. 8. Temperature dependence of the superlattice reflection intensities of $TaD_{0.72}$. I_0 is the intensity at $-166°C$.

HKL	I_{obs}	I_{cal}
011	10.6	11.0
111, 200, 020	} 100.0	41.7
110[b]		58.3
211	9.3	9.8
220, 002	} 58.7	27.6
200[b]		31.4

[a] The model is based on the two-phase mixture of α-$TaD_{0.70}$ and δ-$TaD_{0.75}$. The Debye–Waller factors $B_{Ta} = 0.3\ Å^2$ and $B_D = 1.3\ Å^2$ are used.

[b] Reflections of the α-phase.

that the Ta_4D_3 superstructure transforms to the Ta_2D_{1+x} structure around $-70°C$ at the composition $TaD_{0.72}$.

In the temperature range between -70 and $58°C$ (β_1-phase), the reflections of type II and III are observed, being consistent with the result described in Section 3.1. The abrupt drop in the intensity of the type II reflections at $58°C$ (Fig. 8b) indicates the disappearance of the Ta_2D_{1+x} structure in accordance with the β_1–$(\alpha + \delta)$ transition in the specific heat curve of Fig. 6c.

At temperatures between 58 and 96°C, only the type III reflections are observed. As noted above, the X-ray diffractometry in this temperature range shows the coexistence of the two phases, α and δ. The neutron diffraction data obtained at 80°C can be interpreted by assuming the mixture of six parts of α-$TaD_{0.70}$ and four parts of δ-$TaD_{0.75}$; the former has the random deuterium arrangement in the tetrahedral sites of the bcc metal lattice and the latter possesses the TaD structure (7) with 4 Ta in the $4(f)$ sites and 3 D in the $2(a)$ and $2(b)$ sites of the space group $Pnnn$. As given in Table III, the calculated intensities agree well with the observed

results, R-factor being 0.007. As seen in Fig. 8c, the intensity of the type III reflections shows a kink at the transition point of β_1–$(\alpha + \delta)$, decreases with increasing temperature, and finally disappears at the $(\alpha + \delta)$–α transition point (96°C).

4. Discussion

On the basis of the present study together with the previous neutron diffraction results (5–7), the phase relationship of the Ta–D system in the range $TaD_{0.5}$–$TaD_{0.9}$ is proposed as depicted in Fig. 9. The β_1-phase with the Ta_2D_{1+x} structure exists in the range $TaD_{0.50}$–$TaD_{0.74}$ below 55°C. The β_1–α transformation proceeds through the β_2-phase near Ta_2D, and through the $(\alpha + \delta)$ two-phase region in the deuterium-rich compositions. The δ-phase of the TaD structure extends beyond $TaD_{0.75}$. The transition temperature of δ–α determined by the calorimetry becomes higher with deuterium content, and is smoothly connected to the transition point determined by the previous neutron diffraction work (7), shown by a full circle in Fig. 9. The β_1–δ phase boundary is drawn near $TaD_{0.74}$ taking account of the room-temperature neutron diffraction results of $TaD_{0.72}$ and $TaD_{0.75}$ (6). The two-phase fields $(\alpha + \beta_1)$ and $(\beta_1 + \delta)$ may exist between these phases, though no evidence has been obtained at present.
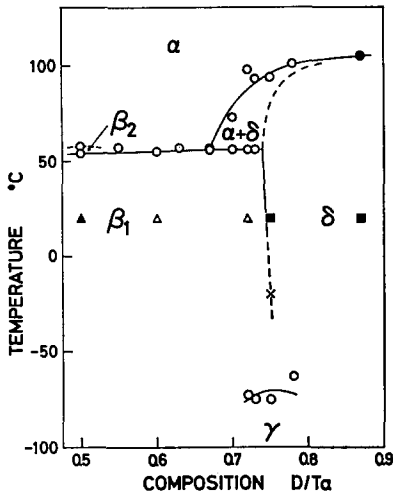
FIG. 9. Phase relationship of the Ta–D system in the range $TaD_{0.5}$–$TaD_{0.9}$. Open circles indicate the phase transition points determined by the calorimetry. Triangles and squares are the phase identifications by neutron diffraction, indicating the existence of the Ta_2D_{1+x} and TaD structures, respectively; △, present work; ▲, Petrunin et al. (5); ■, Somenkov et al. (6, 7); ● and ×, see the text.

As also seen in Fig. 9, the γ-phase of the Ta_4D_3 superstructure is formed below about $-70°C$ from the Ta_2D_{1+x} (β_1) and the TaD (δ) phases in the hypo and hyperstoichiometric compositions, respectively. The critical temperature of Ta_4D_3 ($-20°C$), estimated

from the neutron diffraction work by Somenkov et al. (6), disagrees with the present result. It seems likely, however, that the superlattice reflection studied by them (the index is not given in their paper) may belong to the type II reflections mentioned above, and the transition point may correspond to the β_1–δ phase boundary, as indicated by a cross in Fig. 9.

As noted in Section 3.2, the heat capacity curve of Ta_2D differs from that of Ta_2H reported by Saba et al. (11). For the two thermal anomalies of Ta_2D at 54 and 58°C, the entropy changes are estimated to be 0.40 and 1.6 cal/°, respectively. (The entropy is referred to the alloy containing 1 mole of Ta.) On the other hand, Ta_2H undergoes the phase transitions β_1–β_2–β_3–α at 33, 59, and 60°C, the corresponding entropy changes being 0.35, 1.3, and 0.80 cal/°, respectively (11). Since the β_1-Ta_2H structure is reported to be isomorphic with β_1-Ta_2D (12) and the entropy of β_2-Ta_2H is close to the value for the intermediate phase of Ta_2D (54–58°C), the phase may be termed as β_2-Ta_2D.

In connection with the heat capacity measurement of Ta_2H (11), Wallace (10) has made a neutron diffraction experiment on $TaD_{0.52}$ at 53°C to determine the deuterium positions of the β_2 form. The result has been interpreted equally by either of three models

TABLE IV

ENTROPY CHANGE OF TRANSITION ESTIMATED FROM THE CALORIMETRY (cal/°)

D/Ta	β_1–β_2	β_2–α	β_1–α	γ–β_1	γ–δ	β_1–$(\alpha+\delta)$	$(\alpha+\delta)$–α	δ–α
0.50	0.40	1.6	2.0^a					
0.55			2.3					
0.60			1.9					
0.63			1.9					
0.66			1.6^b			1.1	0.53	
0.70			2.1^b			1.2	0.89	
0.72			1.7^b	0.25		0.58	1.1	
0.73			1.6^b	0.26		0.38	1.2	
0.75				0.39				1.4
0.78					0.43			1.4

^{a} Sum of the values for the β_1–β_2 and β_2–α transitions.
^{b} Sum of the values for the β_1–$(\alpha+\delta)$ and $(\alpha+\delta)$–α transitions.

with disordered and partially ordered deuterium arrangements. In the light of the present study, however, it seems obscure whether the alloy studied by Wallace corresponds to β_2-Ta$_2$D, since this phase exists only in the narrow temperature range of 54–58°C instead of the range 33–59°C for β_2-Ta$_2$H. Structure determination of the β_2 form of Ta$_2$D as well as Ta$_2$H must await further work.

The entropy changes of the transitions estimated from the calorimetry are summarized in Table IV. It is worthwhile to compare these values with the configurational entropy change associated with the deuterium rearrangements, which can be calculated from the structure models described above. A comparison of the β_1–α and δ–α transitions is shown in Fig. 10. In the estimation of the entropy for the α-phase, a perfectly random deuterium arrangement in

the tetrahedral sites (random model) is assumed. The calculated entropy changes are much higher than the experimental results; the configurational entropy of the α-phase is considerably less than that expected from the random model, as pointed out by many workers (11, 13). Next, the entropy of the α-phase is evaluated with a blocking model given by Oates et al. (14), in which partial configurational entropy of the Ta–H system is computed using Monte Carlo methods by the assumption that a hydrogen occupancy of a tetrahedral site excludes the simultaneous occupancy of adjacent sites up to the third nearest neighbours. The calculated entropy changes agree well with the experimental results, as shown by dashed lines. In Fig. 10 a comparison for the γ–β_1 and γ–δ transitions is also shown. The experimental values are somewhat smaller than the calculated results, probably because of the imperfect order of the γ-phase alloys used in the calorimetry.

In conclusion, the neutron diffraction study and the heat capacity measurements on the Ta–D alloys have revealed the deuterium distribution in the ordered phases and the deuterium rearrangement in the order–disorder transformations at the composition TaD$_{0.5}$–TaD$_{0.8}$. It has been seen that the disordering transformation of β_1-Ta$_2$D is not the same as that of β_1-Ta$_2$H.
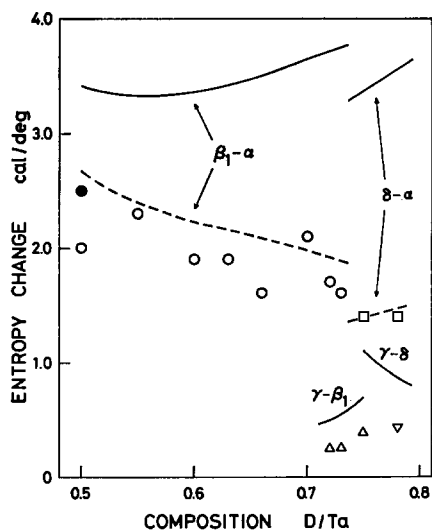
FIG. 10. Comparison of the experimental and calculated entropy changes. ○, □, △, and ▽ represent the experimental results for the β_1–α, δ–α, γ–β_1, and γ–δ transitions, respectively. ● is the result for the β_1–α transition of Ta$_2$H (11). Solid and dashed lines represent the calculated results. For the β_1–α and δ–α transitions, the random model (——) and the blocking model (– – –) are considered for the α-phase. For the γ–δ transition, the excess deuterium atoms in the hyperstoichiometric γ-Ta$_4$D$_3$ are assumed to occupy statistically the 2(d) sites (0 ½ 0, ½ 0 ½).

References

1. T. R. WAITE, W. E. WALLACE, AND R. S. CRAIG, *J. Chem. Phys.* **24**, 634 (1956).
2. B. STALINSKI, *Bull. Acad. Polon. Sci. Ser. III* **2**, 245 (1954).
3. F. DUCASTELLE, R. CAUDRON, AND P. COSTA, *J. Phys. Chem. Solids* **31**, 1247 (1970).
4. V. A. SOMENKOV, *Ber. Bunsenges. Phys. Chem.* **76**, 733 (1972).
5. V. F. PETRUNIN, V. A. SOMENKOV, S. S. SHILSHTEIN, AND A. A. CHERTKOV, *Sov. Phys.-Crysta.* **15**, 137 (1970).

6. V. A. Somenkov, A. Y. Chervyakov, S. S. Shilshtein, and A. A. Chertkov, *Sov. Phys.-Crysta.* **17**, 274 (1972).

7. V. A. Somenkov, A. V. Gurskaya, M. G. Zemlyanov, M. E. Kost, N. A. Chernoplekov, and A. A. Chertkov, *Sov. Phys.-Solid State* **10**, 2123 (1969).

8. M. Hirabayashi, S. Yamaguchi, H. Asano, and K. Hiraga, *in* "Order–Disorder Transformations in Alloys" (H. Warlimont, Ed.), p. 266, Springer-Verlag, Berlin, 1974.

9. H. Asano and M. Hirabayashi, *Phys. Status Solidi (a)* **15**, 267 (1973).

10. W. E. Wallace, *J. Chem. Phys.* **35**, 2156 (1961).

11. W. G. Saba, W. E. Wallace, H. Sandmo, and R. S. Craig, *J. Chem. Phys.* **35**, 2148 (1961).

12. J. Wanagel, S. L. Sass, and B. W. Batterman, *Phys. Status Solidi (a)* **11**, K97 (1972).

13. J. A. Pryde and I. S. T. Tsong, *Trans. Faraday Soc.* **67**, 297 (1971).

14. W. A. Oates, J. A. Lambert, and P. T. Gallagher, *Trans. Met. Soc. AIME* **245**, 47 (1969).